Karlsruhe Institute of Technology

Photonics Lab II

Nanotechnology Lab

Direct Laser Writing and Scanning Electron Microscopy

Supervisor:
MSc. Anne Habermehl

Submitted by:
Tatyana Vuyets - 1911075
Leidy Marcela Giraldo -1911202
Md Shofiqul Islam Khan - 1911257

Contact: shafee.khan@ieee.org

June 8, 2015

Contents

1 Purpose of the experiment

Optical processes are limited by diffraction which can analytically be expressed by the Rayleigh criteria. The aim of this experiment was to introduce us with a cutting edge technique for 3D laser writing beyond the diffraction limit, which nowadays allows an increasing number of applications. Obtaining knowledge of physical principles behind the method, the direct laser writing setup, attaining expertise on using scanning electron microscope and important parameters to characterize the recorded samples were the key training areas of this experiment.

2 Theoretical Background

This Section intends to make an overview and general context about the physical principles behind the experiment done, with the purpose of making comprehensive the obtained results, analysis and conclusions. This section will be divided into two major blocks. Firstly, an introduction through the physical principles related with Direct Laser Writing (DLW) method. Afterwards, an introduction to Scanning Electron Microscopy (SEM) and the relevant parameters for characterization of samples of interest are presented.

2.1 Introduction to Direct Laser Writing - DLW

2.1.1 Resolution Limit

The fundamental restriction of resolution in optical setups using focused beams is dictated by diffraction theory and usually defined by the Airy disc radius and Rayleigh criteria [1, 2] which is expressed by the Eq. 1:

$$r = \frac{1.22\lambda}{2nsin\alpha_{max}} \approx \frac{1.22\lambda}{NA} = \frac{1.22\lambda f}{D}, \tag{1}$$

where λ is the wavelength of excitation, n is the refractive index, α_{max} is the maximum angle of illumination (in microscope $sin\alpha_{max} = 1$), NA is the numerical aperture of an objective with diameter D and focal length f.

From the Airy disc equation is possible to deduce that the better resolution achievable in a given setup depends on how short is the wavelength and how big is the

numerical aperture. However, the choice of the wavelength is limited, because most of the optical components absorb light in the UV range ($\lambda_{min} \approx 350$ nm). And the manufacture of objectives with high-NAs is not a simple task: one microscopic objective includes approximately 10 lenses; the highest NA obtained is around 1.5. To increase this number, microscope immersion technique is used [3].

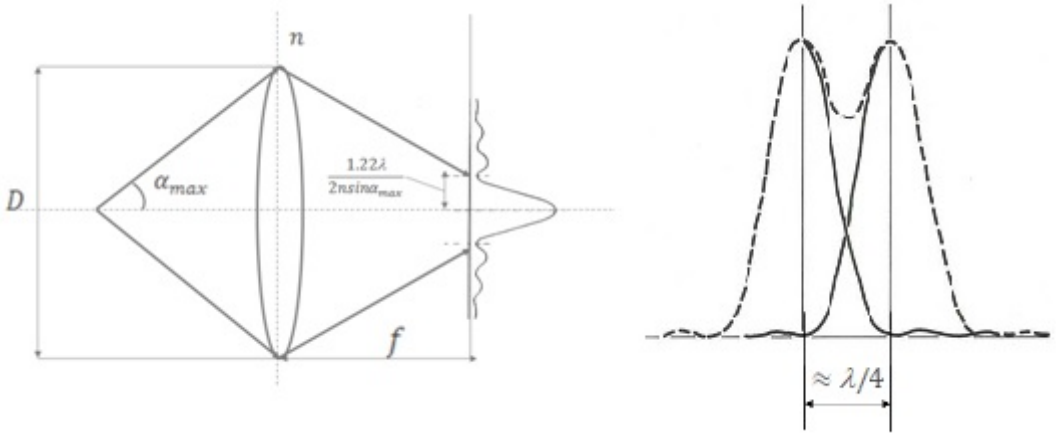

Figure 1: Resolution limit and Rayleigh criteria.

Rayleigh criteria says that two spots are distinguishable between each other as far as the distance between their centers is not less than $\lambda/4$.

2.1.2 Two Photon Polymerization (2PP) and DLW

Two photon Polymerization (2PP) consists in two photon absorption. It is a non-linear process which takes place when high intensities are applied on the medium. In this case the photon density is high enough and the probability that the medium will absorb two photons becomes significant. Two photon polymerization is the base for direct laser writing.

For DLW procedure, near infrared range (NIR) light is used.The same resin materials as in optical lithography are exploited meaning that the chemical structure of the medium is not designed specially for 2PP. Thus, the resin includes photo initiators (PI) or absorbers molecules, which initiate absorption processes. These molecules possess the cross section which enables 1P absorption in a linear regime with UV light exposure. While the energy of one photon from NIR is not enough to cover the band-gap of PI molecules and to be absorbed (see Fig. 2), that is why in a linear regime the resin is transparent for NIR light. By concentrating beams of high

intensities at the resin material, the photon density increases on the focal plane. Hence, the probability of two photon absorption is high enough to be performed. To be able to reach such high photon densities, a pulsed laser is used as an exposure source.

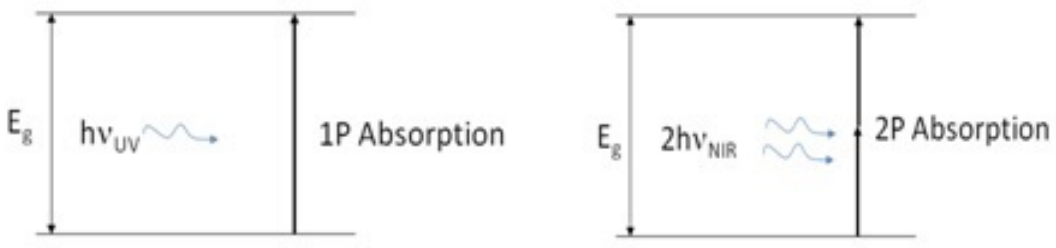

Figure 2: (a) 1PA - One photon absorption. (b) 2PA - Two photon absorption.

The minimum amount of power required to start a 2PP process is called *threshold* which is defined experimentally. It should be noticed that the threshold depends not only on the power of the light source used, but also on the number of pulses applied at the focal plane. By varying the power and number of pulses you can control the volume of polymerized area and even go beyond the diffraction limit. This polymerized volume is usually called voxel (contraction from volumetric pixel). Voxels are bricks from which 3D-structures are built.

Voxel's size gives the resolution of the setup. It depends on several parameters such as the wavefront shape on the focal plane, the relation of refractive indices for the microscope objective immersed and the resin itself [4]. The wavefront shape is important, because the polymerization will occur only in the regions where the concentration of intensity exceeds the threshold and this will define the spot size of writing.

As an example, the Fig. 3 illustrates the prediction curve and measurement data of polymerized volume (diameter) Vs. the average laser power (the irradiation is constant, $t = 40ms$) and as a function of the irradiation time (the laser power is constant, $P_avr. = 30mW$) [7].

As it was mentioned above the resin is transparent for NIR light. This property enables to create 3D-structures in the resin layer by moving a laser focused spot in the medium in all directions (or by moving the sample) and controlling polymerization.

There are two types of 3D-structures drawing called raster mode and vector (or contour) mode. In the raster mode the laser beam goes through all the sample surface "switching on" where it is necessary to create the structure and "switching

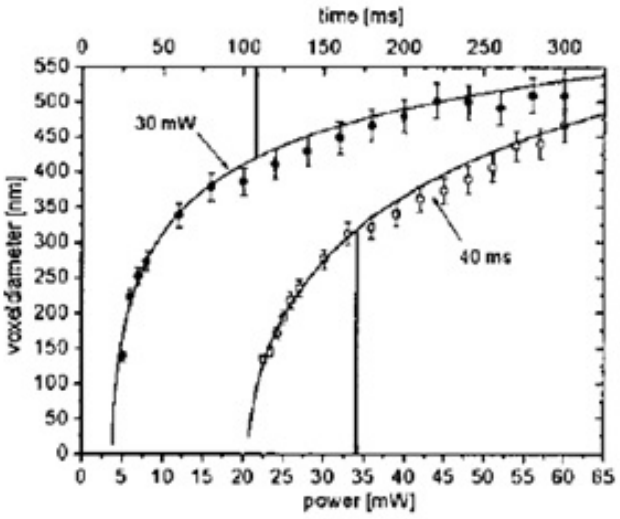

Figure 3: Example of the threshold definition. (Figure taken from [7]).

off" where it is not. "Switching on" and "switching off" are placed in brackets, because it is not a literal switch on/off of a laser system but it means a modulation of the beam. In the vector mode the laser beam is pointed directly at the contour and does not go through the entire sample. Fig. 4 shows the scanning modes.

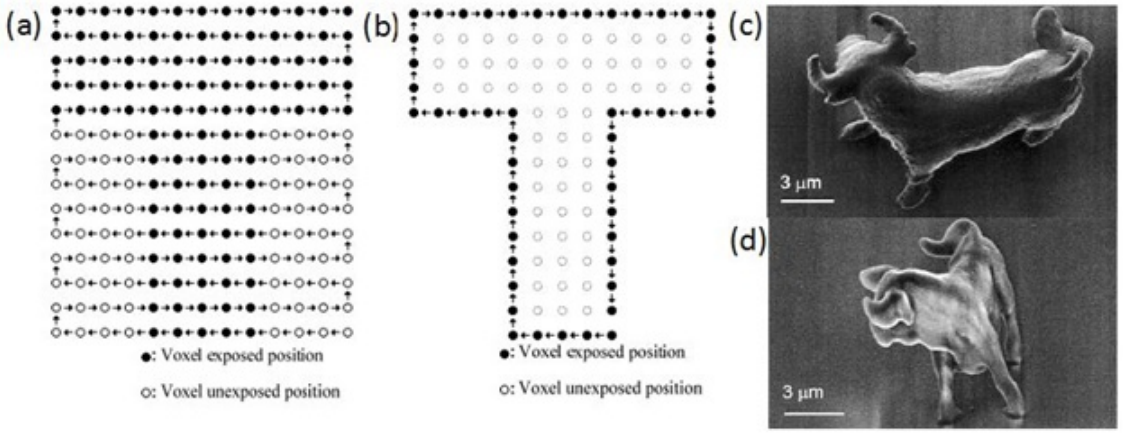

Figure 4: Scanning modes (SM) examples: (a) Raster mode, (b) Vector mode (or contour mode), (c) and (d) SEM images of a micro bull structures using RSM and CSM, respectively. (Figure taken from [5]).

2.2 Scanning Electron Microscope

Due to the limitations in resolution of the traditional optical microscopy and in order to resolve elements with size less than $300nm$, advanced microscopy techniques are commonly used, such as Atomic Force Microscopy – AFM or Scanning Electron Microscopy – SEM [14], which by using other physical principles like the detection of forces between atoms or the wave behaviour of accelerated electrons, respectively, they are able to reach resolutions of few nanometers [10]. Thus, they are convenient and suitable techniques to get information of the topography of nanostructures.

The morphology characterization of voxels, recorded by DLW technique proposed in this report, was made by using SEM technique, whereby, the focus of the next sections will be regarded to it.

2.2.1 Stages and working principle of SEM

The SEM microscopy essentially is composed by four stages as is shown in Fig. 5, a gun chamber, a column electron beam, a sample chamber, an analysis chamber and vacuum pumps.

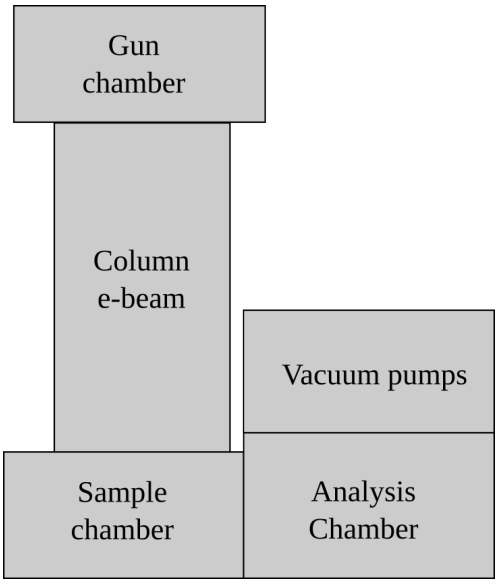

Figure 5: Functional stages of the Scanning Electron Microscope.

The **gun chamber** is the place where the process starts. Electrons with high energy are emitted by thermionic, field-emission or Schottky effect [10]. Figs. 6a and 6b, show a diagram for the first two cases.

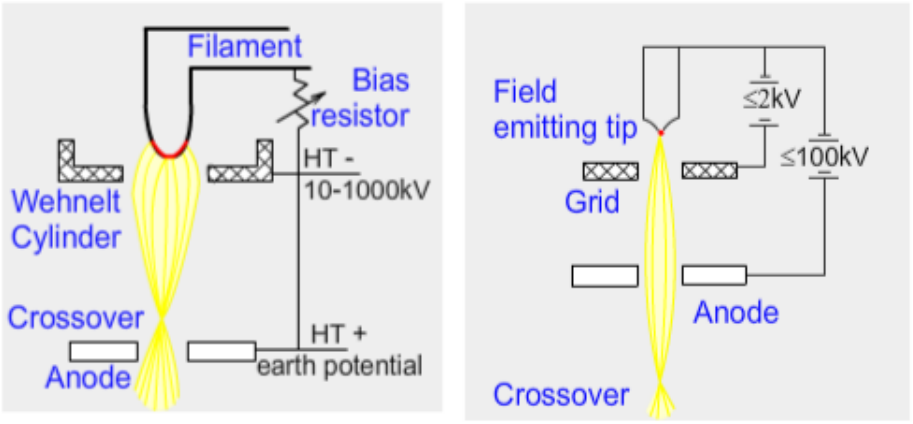

(a) (b)

Figure 6: Gun chambers (a) Scheme by thermionic effect. The filament is heated and when the thermal energy given overcomes the work function of the material, electrons are emitted. Usually the filament is made of Tungsten or Lanthanum hexaboride LaB_6. (b) Scheme by field-emission effect. A tip of tungsten curved usually by etching process is used as a filament. The electrons are emitted by tunnel effect by using a high electric field. (Diagrams taken from [12]).

After the electrons are emitted, a small fraction of them pass though a hole in a positively charged metallic plate called anode, where they are accelerated and converted into a beam in the column of the SEM. These electrons compose the effective source of illumination or e-beam [12], as is shown in Fig. 7.

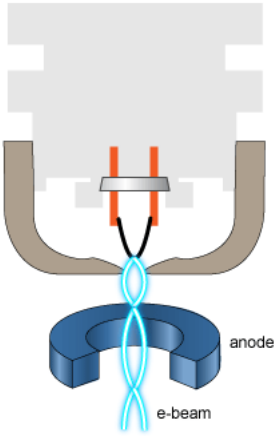

Figure 7: Generation of the effective e-beam. (Diagram taken from [13]).

The quality of the e-beam will be defined by the electric potential difference applied to the anode. It will be a parameter to fix in the microscope because it will influence the resolution. Electron's energies could be set to values between $0.1keV$ to $50keV$ [10].

The e-beam is conducted through the column from the anode until to be focused onto the sample. Fig. 8 shows a transverse section of the column. $L1$, $L2$ and $L3$ are coils, which behave as lenses demagnifying and focusing the electron beam by using the Lorentz force principle, $A1$, $A2$ and $A3$ are apertures which determine the angles of entry or exit of the beam [12, 15]. The scanning coils SC allow the controlled deflection of the beam in order to raster the focused beam over the sample surface point by point, line by line.

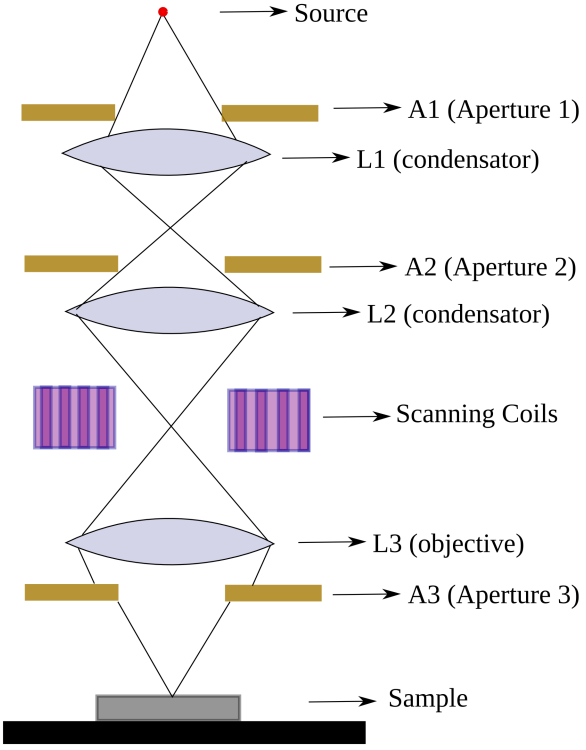

Figure 8: Transverse section of the SEM column. $L1$, $L2$ and $L3$ are electromagnetic lenses. $A1$, $A2$ and $A3$ are apertures. SC are the scanning coils.

With the purpose of increasing the mean free path for the electrons, high vacuum levels are required, thus, scanning electron microscopes usually have two **vacuum pumps**. In first place, a mechanical pump is turn on to reach levels of $\sim 10^{-3}\ Pa$, afterwards, a turbomolecular pump is used to achieve ultra-high-vacuum, even until $\sim 10^{-8}\ Pa$ [10].

As it was mentioned above, the objective $L3$, focusses the e-beam onto the sample, and the accelerated electrons interact with the specimen onto the **sample chamber**. According to the acceleration voltage of electrons, it is created a volume of interaction inside the sample, as is shown in Fig. 9.

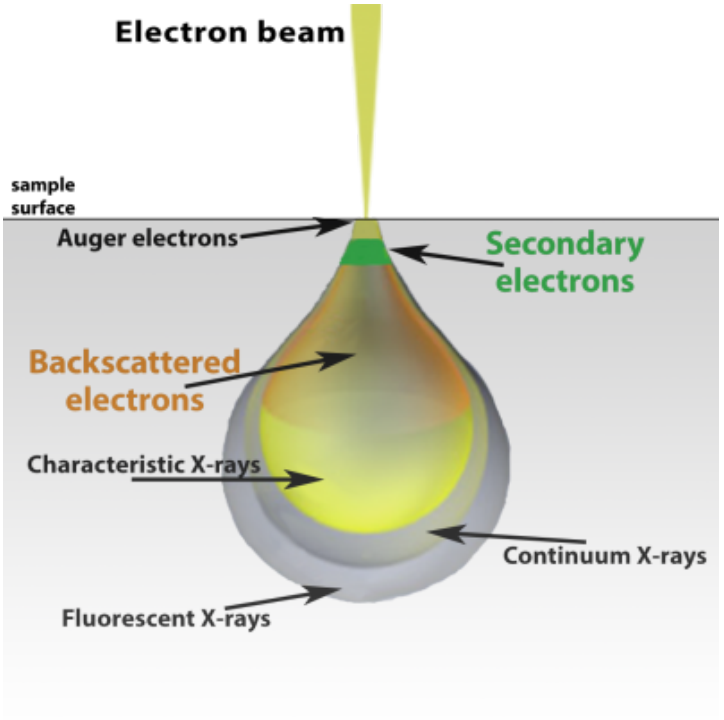

Figure 9: Volume of interaction between the e-beam and the sample (Image taken from [16]).

The interaction between the e-beam and the specimen could produce different effects due to elastic or inelastic scattering of electrons [15]. The elastic scattering produces bouncing electrons which are called back-scattered electrons (BSE). On the other hand, the lost energy by the in-elastically scattered electrons could generate the emission of different ones, like, secondary electrons, X-rays or Auger electrons. All of them give different information from the specimen. Afterwards, they are collected by one or more detectors into the **analysis chamber**. However, the secondary electrons are the most important ones to obtain a SEM micrography.

When the secondary electrons (low energy electrons) are coming off of the sample, they are attracted to a *Everhart-Thornley* detector. This uses a Faraday cage (which prevents possible interferences between the collected electrons and the e-beam) to accelerate the electrons through a scintillator [15] and later those electrons are converted into photons, and by using a light wave guide, they are guided to a

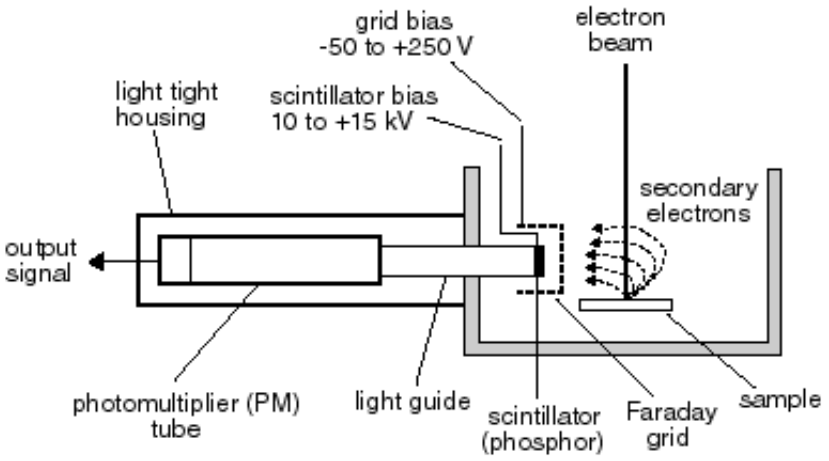

Figure 10: Working principle of the *Everhart-Thornley* detector. (Scheme taken from [18]).

photo-multiplier, where the signal is amplified and the image is generated onto the screen. Fig. 10 shows a scheme of the working principle for a *Everhart-Thornley* detector.

2.2.2 Characteristics of SEM

The main characteristics of a Scanning Electron Microscope are:

1. High resolution (4 to 20nm according to the microscope).
2. Magnification since 10x to 100.000x
3. High depth of focus (stereoscopic image).
4. It gives morphological information.
5. Samples should be compatible with high-vacuum and be conductive.
6. Only can be observed death specimen for the case of biological samples.
7. The micrographies are black and white.

The resolution can be improved by decreasing the spot size which depends on how small is the final aperture in the e-beam column, a high acceleration voltage and a small working distance [15]. The depth of focus (at a fixed magnification) can be enhanced by increasing the working distance and reducing the size of the final aperture [15]. Thus, there is a commitment relation between the depth of focus and

resolution, which should be tested and optimized for each sample in order to achieve a good image.

2.3 Characterization of Voxels

From [7] we can estimate the size of the voxel. Voxel diameter can be estimated as:

$$d(N_0, t) = r_0[\ln(\sigma_2 N_0^2 n \tau_L / C)]^{1/2}, \tag{2}$$

$$C = \ln[\frac{\rho_0}{\rho_0 - \rho_{th}}],$$

where $n = vt$ is the number of pulses, v is the laser pulse repetition rate, t the total processing irradiation time; τ_L is the laser pulse duration; σ_2 is the effective two-photon cross section for the generation of radicals $[cm^4 s]$; ρ_0 is the primary initiator particle density and ρ_{th} is the threshold. r_0 is the standard deviation of the Gaussian light distribution in the main maximum at the focal plane.

The voxel length is determined by the following equation:

$$l(N_0, t) = 2z_R[(\ln(\sigma_2 N_0^2 n \tau_L / C))^{1/2} - 1]^{1/2}, \tag{3}$$

where z_R is the Rayleigh length. To compare equation **??** with equation **??** N_0 can be replaced as follows:

$$N_0 = \frac{2}{\pi r_0^2 \tau_L} \frac{PT}{v\hbar\omega_L}$$

where P is the average laser power and T is the fraction of light transmitted through the objective.

3 Experimental setup and Procedure

3.1 Experimental Setup

The experimental setup for DLW is presented in Fig. 11. A Ti:Al2O3 laser beam pass through a motorized neutral density filter which allows to control the exposure

over the sample. The beam is expanded with a lens, filtered with a pinhole and then is collimated with the second lens and redirected by using a mirror through an optical microscope with immersion apochromat objective, in order to increase the numerical aperture.

Numeric values for the wavelength, magnification, pulse duration and pulse repetition and numerical aperture are detailed on the Fig. 11.

In this setup for 3D-structures writing the sample is placed onto the 3-axis nanometer positioning table and moved in accordance with the structure shape.

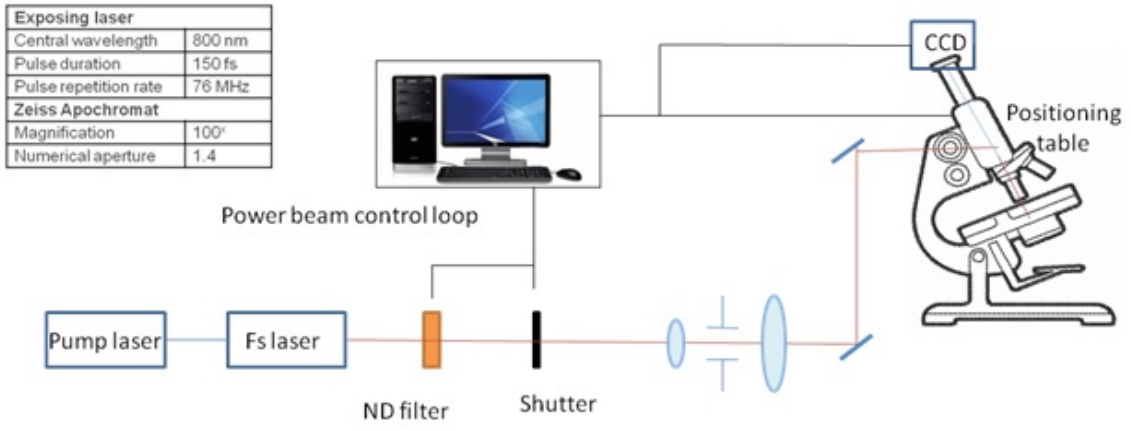

Figure 11: Experimental setup for DLW.

3.2 Sample Preparation

The sample was prepared before the experiment day. Sample preparation is explained briefly in the following sections.

3.2.1 Substrate Cleaning

Glass sample was cut into a square piece to use as substrate. Before preparing the sample it was cleaned using acetone and isopropanol in ultrasonic bath.

3.2.2 Spincoating

After cleaning the substrate it was spincoated to create a layer of photoresist resin SU8-2050. Spincoating began with a speed of 500 rpm for 10 seconds so that the resin is spread uniformly all over the substrate. Afterwards spincoated at 3000 rpm for 30 seconds to obtain desired thickness of the resin.

3.2.3 Soft Bake

Spincoated substrate was then put on the hotplate for 8 minutes at the temperature of 95^0C to remove the remaining solvent from the substrate.

3.2.4 Exposing Photoresist by DLW

Photoresist was exposed by the direct laser writing setup. Desired structure was printed in the resin with the exposure of laser light.

3.2.5 Post Exposure Bake

The exposed sample is then again put on the hotplate for post exposure bake this time for 8 minutes at the temperature of 85^0C. Purpose of this bake is to harden photoresist and strengthen the designed structure before the development process.

3.2.6 Development of Exposed Sample

After post exposure bake the sample was developed using the devloper mr-Dev 600. After the development of substrate unexposed area of the photoresist is expected to go away.

3.2.7 Hardbake

Developed sample is then hard baked on hotplate for 1 hour at the temperature of 120^0C to removed all the solvents and make the structure very strong.

3.2.8 Sputtering

To observe and characterize the sample was sputtered with gold coating in the sputtering machine. In order to obtain high resolution visibility in the Scanning electron microscope monolayer of gold is required in the sample surface.

3.3 Unattended SEM practice

An unattended practice was done inside the cleanroom at Light Technology Institute – LTI after the proper instruction from the supervisor, in order to practice how to set the values of acceleration voltages of the e-beam, the depth of focus, magnification and changing between scanning modes with samples with different sizes.

It is important to note that all the measured structures in the unattended practice were micrometric. The experimental challenge was higher, to resolve structures with hundreds of nm like the voxels written by DLW.

3.4 Characterization of Exposed Structure

In this step, the polimerized sample was observed with SEM and the necessary measurements were done to understand the voxel size dependence on different parameters were performed.

4 Result Analysis

In this section results obtained during the experiment are presented. First two subsections discuss the our practice session with the SEM where microstructures were observed. This session was intended to prepare ourselves to be able to observe nanostructures and characterize direct laser written voxels.

4.1 Observing the Bee

Biological samples coated by magnetron sputtering technique with a gold thin film were observed and analyzed under the microscope. Fig. 12 shows the results for a bee's eye with different magnifications between $45x$ to $750x$. The hexagonal structure

of the eye starts to be resolved at $180x$ but it could be measured with more accuracy at $750x$. The wide and length obtained were $35.35\mu m$ and $19.74\mu m$, respectively.

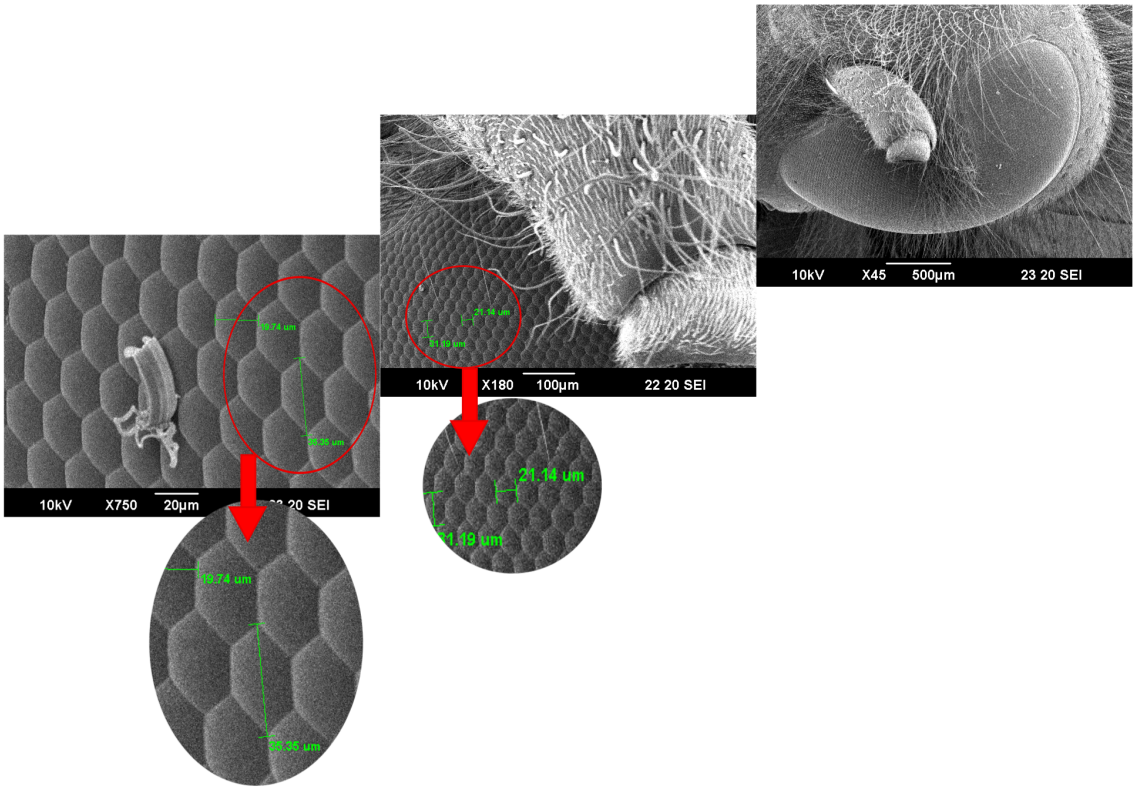

Figure 12: Experimental SEM images of a bee's head-eyes using $10kV$ and different magnifications ($45x$, $180x$ and $750x$).

4.2 Observing the Butterfly

On the other hand, Fig. 13 shows the results for a butterfly's wing. Without using any microscope device, the butterfly wing looks like a solid structure, but by using a SEM and increasing the amount of acceleration voltage for the electrons, the pattern starts to be resolved, and it reveals a very sharp shape with a period of 1.58μm, approximately, applying $20kV$.

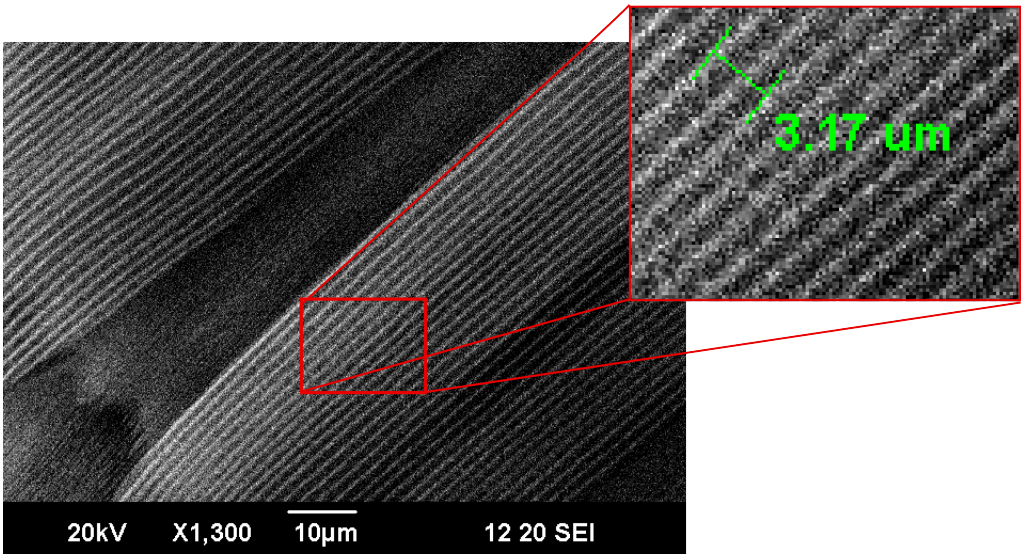

Figure 13: Experimental SEM image of a butterfly wing using $20kV$.

4.3 Observing the LTI logo

On the sample substrate there was a Light Technology Institute - LTI logo which is observed by SEM. To explore that logo first we focused on the top of the logo which initially seemed to be a point from the top. Afterwards we rotated the sample holder of SEM by 45^0 and then again refocused to the aforementioned point as depicted in Fig. 14.

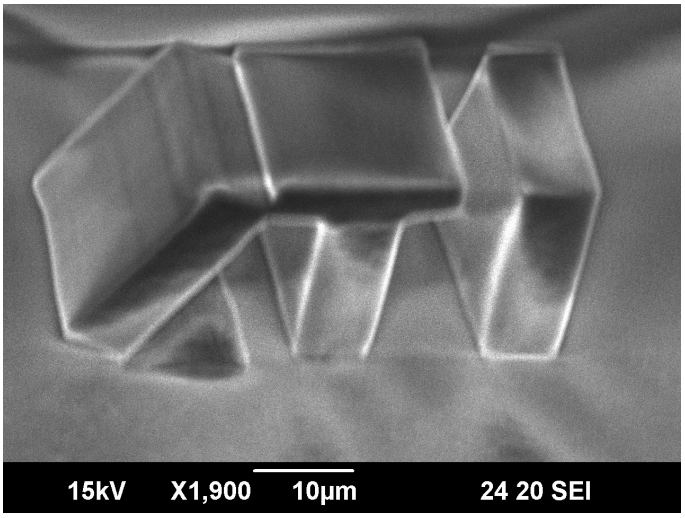

Figure 14: Experimental SEM image of the LTI logo.

4.4 Voxels Characterization

In the sample substrated there were several blocks of voxels e.g. first block in Fig. 15. During our measurement we considered only first three voxel blocks. Each voxel block consisted of seven lines where each line corresponded to exposure time of 50 ms, 40 ms, 30 ms, 25 ms, 20 ms, 15 ms and 10 ms. Each blocks were prepared with different irradiation power of 15 mW, 1.3 mW and 1.1 mW.

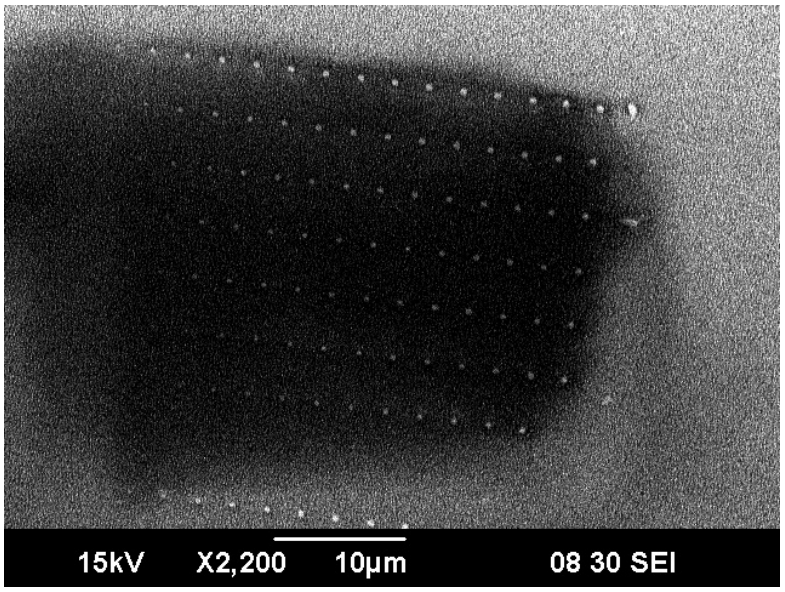

Figure 15: SEM picture for voxel Block 1 where irradiation power used was 1.5 mW

To characterize our samples we needed to measure the voxel length and diameter. To calculate the voxel length we counted the number of voxels in each line of Voxel blocks. During this process we ignored the last bigger elliptical voxel which is supposed to be fallen voxel (Fig. 16a). We counted number of voxels leaving the fallen one. Since in each line for a constant exposure time the beam focus was moved 100 cm from consecutive voxels during the polymerization proces, total number of voxels multiplied by 100 nm gives the voxel length for each line.

We have calculated voxel length for each seven lines of three different power irradiated blocks. But to determine voxel diameter we only took measurement from the first block due to the time constraint of the experiment. In this step we measured the diameter of the last two voxels of each line (ignoring the fallen one) as depicted in Fig. 16b.

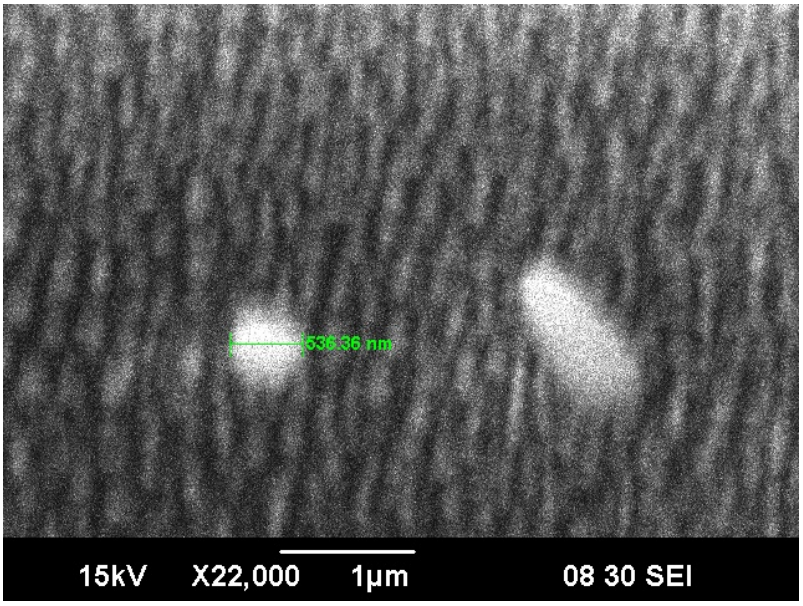

(a) Last two voxels of the 1^{st} line.

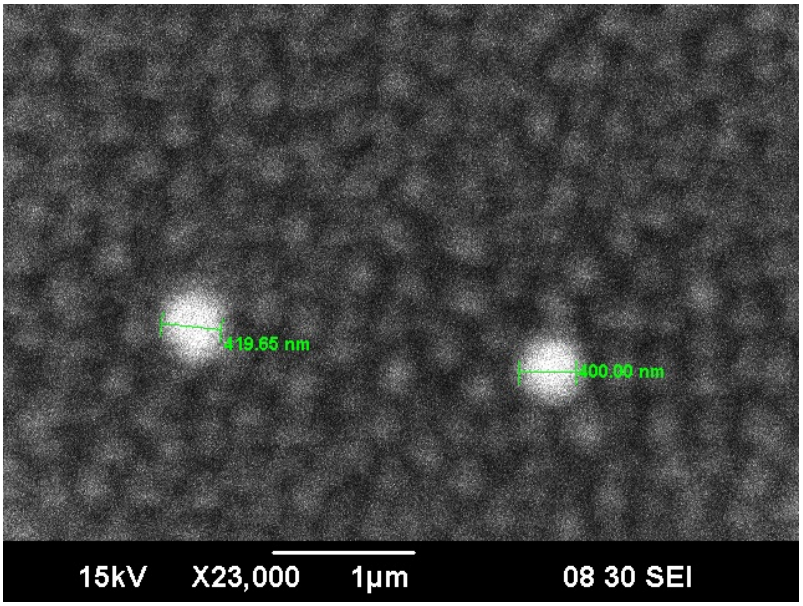

(b) Last two voxels of the 6^{th} line.

Figure 16: Magnified SEM images of Block 1.

Then we took the average of the two diameters and obtained voxel diameter for different exposure time. Multiplying the irradiation power with exposure time we

found the laser pulse power and obtained power versus voxel diameter curve as in 17. In the inset of Fig. 17 we also include the experimental data from [6] which is in agreement with our characterization data.

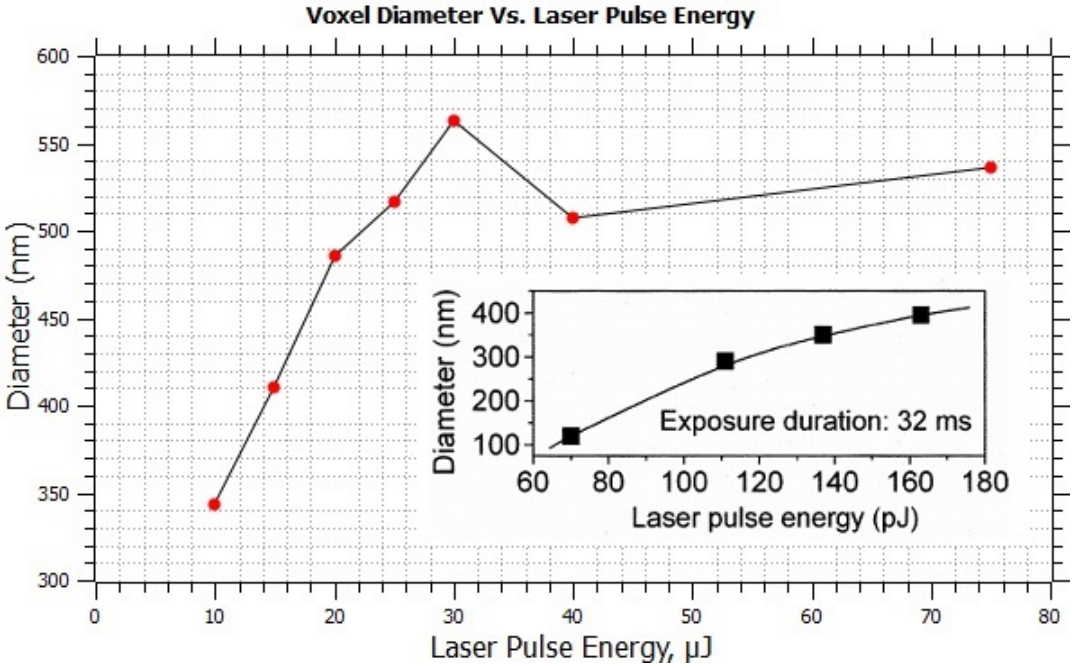

Figure 17: Diameter of voxels with respect to the laser pulse energy. (Inset: Data from reference [6]).

In the Fig. 18 we have presented the voxel length dependence on exposure time (figure 18a) and on irradiation power (Fig. 18b). Length vs exposure time data was presented for different exposure powers and length vs power curve was plotted for different exposure times. These family of curves give a great insight to the voxel size dependence on exposure and power.

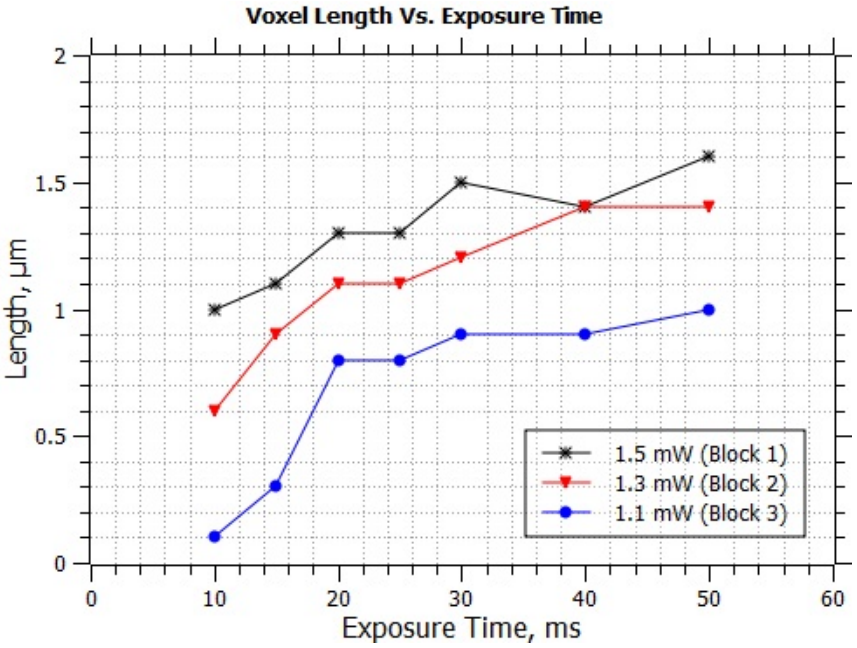

(a) Length Vs. Exposure Time.

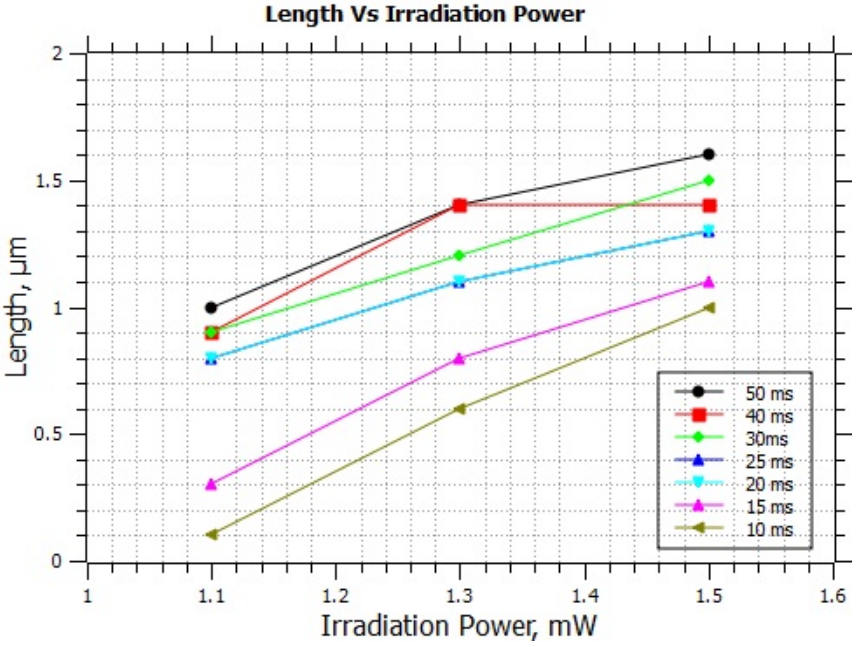

(b) Length Vs. Irradiation Power.

Figure 18: Effect of exposure time and irradiation power on voxel length.

5 Conclusions

After this experiment we have obtained a clear vision on two photon polymerization process, direct laser writing method and expertise in using SEM. The characterization process that we have learned in [7] and [6] has been practically implemented in this experiment. However, there was some malfunction of SEM during the experiment which costed us a mentionable amount of time. Otherwise we would be able to extract diameter data from other two voxel blocks. Some process data for the sample were unknown as we did not prepare the sample by ourselves. If known, then experimentally obtained data could be compared with equation 2 and equation 3 to achieve deeper insight to the measured data.

Acknowledgements: These results were obtained in the framework of a DLW laboratory, under the supervision of MSc. Anne Habermehl at Light Technology Institute - LTI, as part of the MSc. in Optics & Photonics program, from Karlsruhe Institute of Technology, Germany. Special thanks to Ruben Huenig from LTI in the troubleshooting of SEM.

References

[1] G. B. Airy. On the Diffraction of an Object-glass with Circular Aperture. Transactions of the Cambridge Philosophical Society, Vol. 5, p. 283-291, (1835).

[2] F. E. C, Culick. A Note on Rayleigh's Criterion. Combustion Science and Technology, 56 (4-6). pp. 159-166, (1987).

[3] S. F. Gibson, and F. Lanni, Experimental test of an analytical model of aberration in an oil-immersion objective lens used in three-dimensional light microscopy. JOSA A, 9(1), 154-166.

[4] M. Thiel and M. Hermatschweiler. Three-dimensional laser lithography. Optik & Photonik, 6. pp 36–39, (2011).

[5] A. Spangenberg, N. Hobeika, F. Stehlin, J. P. Malval, F. Wieder, P. Prabhakaran, P. Baldeck and O. Soppera. Recent Advances in Two-Photon Stereolithography *InTech: Nanotechnology and Nanomaterials» "Updates in Advanced Lithography"*, (2013).

[6] H.B. Sun and S. Kawata, Two-Photon Laser Precision Microfabrication and its Applications to Micro-Nano Devices and Systems. *Journal of Lightwave Technology*, Vol 21, 3, pp. 624, (2003).

[7] J. Serbin, A. Egbert, A. Ostendorf, B. N. Chichkov, R. Houbertz, G. Domann, J. Schulz, C. Cronauer, L. Fröhlich, and M. Popall. Femtosecond laser-induced two-photon polymerization of inorganic–organic hybrid materials for applications in photonics. *Opt. Lett.*, Vol 28, 5, (2003).

[8] A. Ostendorf and B. N. Chichkov. Two-Photon Polymerization: A New Approach to Micromachining-Femtosecond lasers enable microfabrication with resolution beyond the diffraction limit. *Photonics Spectra*, Vol 40, 10, pp. 71, (2006).

[9] D.S. Engstrom, B. Porter, M. Pacios and H. Bhaskarana. Additive nanomanufacturing - A review. *J. Mater. Res.*, Vol 29 , 17, pp. 1792, (2014).

[10] L. Reimer and PW. Hawkes. Scanning Electron Microscopy: Physics of Image Formation and Microanalysis. *Springer Series in Optical Sciences*, (2010).

[11] Scanning Electron Microscope. [Online] *http://www.matter.org.uk/tem*, (04 June 2015).

[12] Matter - University of Liverpool. Introduction to Electron Microscopes. [Online] *http://www.materials.ac.uk/elearning/matter/*, (04 June 2015).

[13] Australian Microscopy and Microanalysis Research Facility. Scanning Electron Microscopy in practice. [Online] *http://www.ammrf.org.au/myscope/sem/practice*, (04 June 2015).

[14] V. Kazmiruk. Scanning Electron Microscopy. *InTech*, (2012).

[15] B. Hafner. Scanning Electron Microscopy Primer. *Characterization Facility, University of Minnesota—Twin Cities*, (2007).

[16] Nanoscience Instruments SEM Components [Online] *http://www.nanoscience.com/products/sem/technology-overview/sample-electron-interaction/*, (04 June 2015).

[17] A. Habermehl. Laboratory Nanotechnology – Experiment: Direct laser writing and Scanning electron microscopy. *Lab Guide, Ligth Technology Institute (KIT)*, (2015).

[18] Secondary Electron Imaging. GLG 510 – Course Overview. [Online] *https://www4.nau.edu/microanalysis/Microprobe/Imaging-SEM.html*, (04 June 2015).